Jestr

Journal of Engineering Science and Technology Review 15 (5) (2022) 22 - 31

Research Article

JOURNAL OF
Engineering Science and Technology Review

www.jestr.org

Analysis on Membrane-Stubble Separation Device under the Action of High-Voltage Electrostatic Adsorption

Zaibin Wang[1,2], Xufeng Wang[1,2], Jianfei Xing[1,2,*], Can Hu[1,2,3] and Xuanfu Li[1,2]

[1]*College of Mechanicaland Electrical Engineering, Tarim University, Alar 843300, China;*
[2]*College of Engineering, China Agricultural University, Beijing 100083, China;*
[3]*Modern Agricultural Engineering Key Laboratory at Universities of Education Department of Xinjiang Uygur Autonomous Region, Tarim University, Alar 843300, China*

Received 29 June 2022; Accepted 18 November 2022

Abstract

The application of plastic film mulching technology provides good soil growth ecology for the growth of cotton and other crops. However, the plastic film residues also cause residual film pollution in cotton farming areas, destroying the physical quality of the soil and affecting the growth of crops. At present, China mainly adopts the method of mechanical recycling to recover the residual film, but the resulting film has a high impurity rate and is mixed with a large amount of crop residues, making secondary recycling difficult. To solve this problem, a membrane stubble separation device under the action of high-voltage electrostatic adsorption was designed in this study. Maxwell software was used to conduct simulation analysis and experimental research on the separation device, and the Design-Expert® software was used to optimize analysis and explore the influencing factors and specific processes of the membrane-stubble mixture during the separation process. Results show that the static voltage level, the fragmentation degree of the residual film, the charged area of the electrode plate, and the distance between the electrode plate and the separation roller all have significant effects on the separation rate. In terms of optimizing the results, when the static voltage level is +54.60 kV, the residual film size is 21.75 cm^2, the height between the electrode plate and the separation roller is 78.8 mm, and the rotation speed of the separation roller is 31.30 r/min, the best separation efficiency can be obtained, with a separation rate reaching 79.15%. The obtained conclusions provide a significant technical reference for solving the problems of difficult separation of membrane impurity and high impurity content in mechanically recovered residual membrane mixtures.

Keywords: Residual film recovery, Electrostatic separation, Membrane stubble separation device, Optimization simulation

1. Introduction

Plastic film mulching technology plays a variety of important roles in the process of crop planting and growth, such as increasing temperature and moisture, moisturizing and retaining water, preventing pests, and inhibiting the growth of weeds [1-3]. However, due to the lack of effective plastic film recycling methods, large amounts of waste plastic film remain in the soil environment, thus affecting the quality of farmland soil [4]. Furthermore, waste and residual film may decompose microplastics in the soil and be absorbed by crops, thereby affecting crop growth [5-7]. The "Agricultural Film Recycling Action Plan" issued by the Chinese Ministry of Agriculture in 2017 [8] also emphasized the prevention and control of farmland residual film pollution as well as the importance and the necessity of improving the utilization level of waste agricultural film. In the arid planting areas of Northwest China, mechanized residual film recycling operation is mainly carried out by using a residual film recycling machine—an important means of controlling the residual film pollution problem [9]. Wen Haojun [10] of Shihezi University designed a second-order chain plate-type straw-crushing plastic film recycling machine. Jin Wei [11] of Xinjiang Agricultural University developed a spring tooth-type residual film recovery machine, while other scholars have also conducted numerous studies on the mechanized recovery of residual film. However, at present, many impurities can still be found in residual films recovered by mechanical recycling. In particular, recovered residual films in plough layers still contain mixed impurities, such as crop residues and gravel soil. Among several advantages, the physical properties of such film stubble mixtures ware difficult to accurately measure, the cost of reprocessing into plastic particles was high, and the recovery technology and secondary utilization ware highly difficult [12-14]. Therefore, finding an effective method to separate the membrane-stubble mixture can help lower the impurity content of the residual membrane, reduce the technical difficulty and cost of processing and reuse, and improve the economic benefits of recycling residual membranes, which in turn, can effectively solve the problem of the secondary pollution of residual membrane [15,16].

At present, the electrostatic removal of impurities and separation technology has been applied in many industries [17-19]. In addition, Dizdar [20] used friction charging to achieve mineral separation and investigated whether mineral separation can be carried out under the influence of different influencing factors and materials of the conveyor belt. The friction charging method can reach up to +35 kV. The separation test showed that the friction charging method can realize the separation of minerals. Richard [21] studied the application of roller electrostatic separators for the separation of conductive and non-conductive components in particle mixtures. Experimental studies showed that 75.00%

*E-mail address: 591101353@qq.com
ISSN: 1791-2377
doi:10.25103/jestr.155.04

of aluminum particles and 99.97% of PVC can be removed, resulting in copper with a purity of 98%. Kawamoto [22] designed a flat-plate conveyor consisting of parallel electrodes to separate particles by size under the action of a voltage of an appropriate frequency. Medles [23] found that the size of plastic particles had a significant impact on the separation efficiency in the process of electrostatically separating plastic particles. Jędryczka [24] developed an automatic test bench for electrostatic separation of plastic waste, equipped with a computer vision system for real-time monitoring of separation efficiency. Louati [25] determined the effect of electrostatic voltage level and air gap thickness on the electric adhesion of metal and plastic through numerical simulation and verified the feasibility of metal-plastic mixture separation.

Studies on the application of high-voltage electrostatic in the agricultural field have continued to increase every year [26-28]. For example, Julián Sánchez [29] used an electrostatic hand-held sprayer and a traditional hand-held sprayer to spray medicines on greenhouse vegetables. The results showed that the spraying effect of the electrostatic spray was improved compared with the hand-held spray gun. Dascalescu [30] used a belt-type corona separator to charge the wheat bran and found that the freeze-dried samples retained the charge better than the samples without the freeze-drying process, thus sorting out the wheat bran with high nutritional value. Wang [31] used a grinding device and an electrostatic sorting device to extract protein from seeds, achieving a high ground powder protein content of 65.37%, which broadened the idea for the development of grinding technology. The problem of membrane impurity separation is the main reason for the difficulty behind the secondary recycling of residual membranes. The above studies have shown the feasibility of using electrostatic adsorption technology in separating residual membranes and impurities, thus providing theoretical and technical support for membrane-stubble separation under the action of high-voltage static electricity.

To address the lack of effective and scientific separation technology of membrane-stubble mixture after mechanical recovery and the difficulty of the secondary recovery of residual membrane, this study proposes and develops a membrane-stubble separation device under the action of high voltage electrostatic from the perspective of practical agricultural engineering application. In this work, we used Maxwell to simulate and analyze the charge of the residual membrane in the adsorption electric field of the device. Then, we designed experiments to study the separation effect of the membrane-stubble mixture under different conditions and determined the device parameters when the optimal separation effect is achieved. Using the device to separate and recover the residual film and impurities can help enterprises reprocess and utilize residual films, reduce the problem of secondary pollution of residual films, and provide a reference for the mechanized control of the residual film pollution, thus promoting the sustainable development of agriculture.

2. Materials and methods

2.1 Analysis of the film-stubble mixture

A film-stubble mixture is the mulch film recovered by the residual film recovery machine. According to the literature, the current impurity content after the operation of the residual film recovery machine is about 10%-25% [32-34], the film-stubble mixture mainly includes residual film, clods, sand and gravel, and crop residues. In this experiment, cotton plots in Southern Xinjiang were selected, and the sampling locations were as follows: Xingfu Farm, Alar City, First Division of Xinjiang Production and Construction Corps, Shule County, Kashgar Region, Xinjiang Uygur Autonomous Region, Kuqa County, Aksu Region, Bayingoleng Mongolian Autonomous Prefecture, and Korla Region. Bohu County had a total of five sampling sites. The sampled plot was a cotton field, and the film covering period was more than 10 years. The plot area was more than 1 hm^2, and the residual film was recovered by mechanical film collection. The sampled products are representative. The sampling period was after the autumn harvest in November 2021.

The field film-stubble mixture sampling method was as follows: first, the residual films were recovered by the residual film recovery machine after selecting one cotton field for each sampling area and taking two samples from each cotton field. The film-stubble mixture was collected into the sample bag, which was marked with a signature pen to facilitate subsequent processing. A total of 10 samples were collected at the end of sampling in five areas. The collected samples were preliminarily cleaned and pulverized. After cleaning, they were dried and weighed, and their area distribution was counted. After Origin treatment, the area distribution of the fragmented residual film was obtained, as shown in Fig. 1.

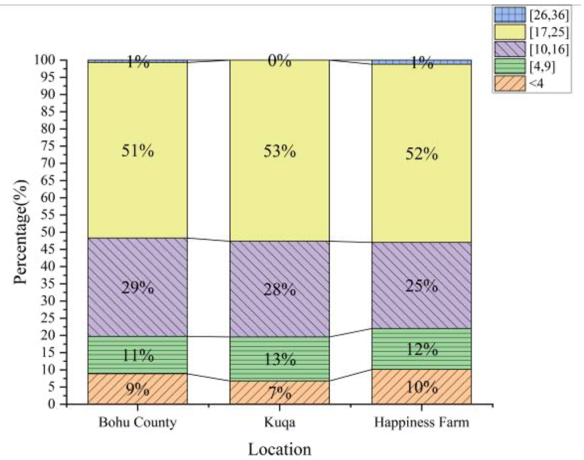

Fig. 1. Framer membrane distributed diagram

2.2 Design and construction of the test device

The membrane-stubble separation device is composed of a high-voltage electrostatic generator, separation roller, electrode plate, motor, conveyor belt, film brush, collection box, and other components. During the operation of the device, the high-voltage electrostatic generator is connected to the electrode plate through a wire and discharges the small contact surface; the output voltage is a positive voltage. The electrode plate with static voltage will charge the residual film, and the residual film with a positive charge will be adsorbed on the separation roller under the action of the electrostatic field. The separation roller is powered by a servo motor with a speed adjustment range of 1-3000 r/min. The residual film mixture passes through the conveyor belt to the top of the separation roller. When the separation roller rotates, the residual film mixture is affected by electric field force, gravity, and centrifugal force. Due to the varying adsorption effects of different materials, impurities will fall into the collection box at the side of the high-voltage electrostatic generator under the influence of the above forces. As the residual film is light and charged, the residual film will continue to be adsorbed on the separation roller and then brushed off into another film collecting box through the film brushing part. The structural diagram of the membrane residue separation device is shown in Fig. 2.

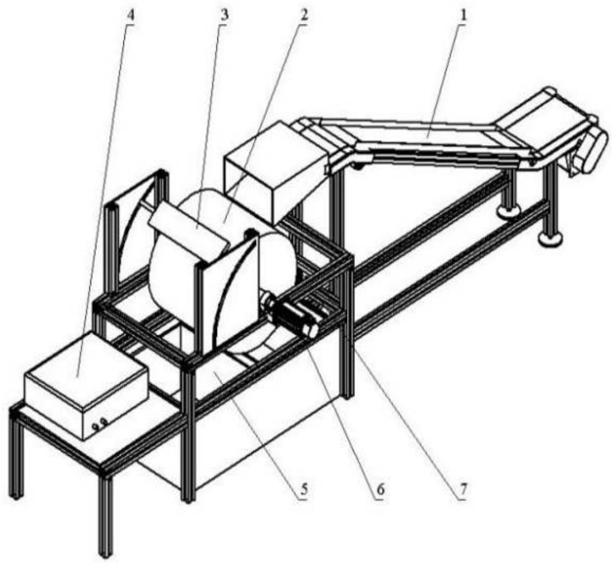

1. Conveyor belt 2. Separating roller 3. Electrode plate 4. High voltage electrostatic generator 5. Collecting box 6. Motor 7. Residual film brush
Fig. 2. Structural diagram of membrane stubble separation device under high voltage static electricity

The high-voltage electrostatic generator is the core component of the separation device. It consists of two parts: an electrostatic emission rod and a DC high-voltage power supply. The DC high-voltage power supply can add a high voltage to the electrostatic emission rod, and then the electrostatic emission rod charges the experimental object by emitting charged ions.

By analyzing the field strength between the electrode plate and the separation roller, we have:

$$E = \frac{u}{d} \tag{1}$$

The capacitance of the electrode plate is expressed as:

$$C = \frac{q}{u} = \frac{\sigma S}{\sigma d} = \frac{\varepsilon_0 S}{d} \tag{2}$$

where C represents the capacitance, d represents the distance between the electrode plate and the separation roller, S represents the cross-sectional area, q represents the coulomb, and U represents the voltage.

The voltage electrostatic adsorption power supply model is PW-P104-8ACF1 (Wendong High-voltage Electrostatic Generator). The power is 200 W, and the power supply has over-voltage, over-current, and short-circuit protection to ensure the safe and smooth progress of the test. During the test, the high-voltage electrostatic measuring instrument was selected as follows: SIMCO-FMX-003, measurement range = -200 to +200 kV, measurement accuracy = 0.1 kV.

The main technical parameters of the high voltage electrostatic separation device are shown in Table 1 below.

Table 1. Main technical parameters of the unit

Design index	Measure	Value
Device size	m	2.2×0.5×1.25
Working speed of separating roller	RPM	1~50
Motor speed	RPM	20~1000
Static voltage range	kV	30~65
Conveyor speed	m/s	0.3

The film collecting box was designed as a drawer in which the residual films and impurities were cleaned and classified. A layer of insulating rubber pad was laid under the device to prevent accidental injury to the test personnel due to leakage during the experiment. The completed membrane-stubble separation device under the action of high voltage electrostatic is shown in Fig. 3.

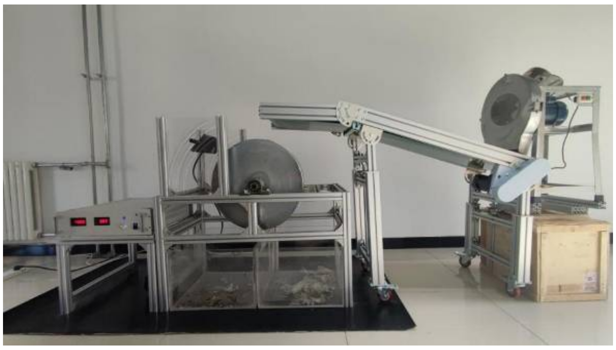

Fig. 3. Separation device physical diagram

2.3 Simulation test of high-voltage electrostatic residual film adsorption electric field

To study the separation method of membrane stubble under high-voltage static electricity, the distribution of electric field and the force of residual membrane in the electric field should be analyzed first. The static voltage level of the device, the height of the electrode plate, the size of the residual film, and the speed of the motor ware selected as influencing factors through the separation principle of high-voltage static electricity and the reference to the literature. Then, the Maxwell electric field simulation software was used to simulate the electric field distribution between the separation devices. The drawn 2D and 3D models of electrode plates and separation sticks were imported from Solidworks into Maxwell to ensure the authenticity of the field strength distribution and vector distribution of the simulated electric field. The parameters of Maxwell software are shown in Table 2.

Table 2. Maxwell parameter setting table

Option	Parameter
Maxwell solver	Electrostatic field
Electrode plate material	Graphite
Separation roller material	Steel
Boundary conditions	Air
Voltage Excitation	55 KV
Maximum Number of Passe	10
Percent Error	1 %
Refinement Per Pass	30 %

Once the setting is completed, the model was automatically meshed according to the set times and accuracy, and the operation detection and solution were carried out to obtain the inter-plate electrode field strength distribution diagram and the inter-plate electrode electric field vector distribution diagram. The analysis showed that the electric field force when the residual film was charged changed with the change of the electric field strength, thus directly affecting the separation efficiency of the mixture.

Therefore, the field intensity distribution between the electrode plates of the separation device was studied, and the changes of the electric field intensity under different conditions were analyzed. Maxwell was used to set the following four conditions for simulation:

(1) Change the applied electrostatic voltage level and study the electric field distribution and vector direction between the two electrode plates under different electrostatic voltage levels.

(2) Change the distance between the electrode plates and study the magnitude of the static voltage level and the electric field vector distribution of the two electrode plates at different distances.

(3) Change the thickness of the electrode plate and study the magnitude of the charged voltage and the vector distribution of the other electrode plate under the condition of different thicknesses of the electrode plate.

(4) Change the width of the electrode plate and study the magnitude of the charged voltage and the vector distribution of the other electrode plate under the condition of different widths of the electrode plate.

2.4 Regression experimental design

The high-voltage electrostatic membrane impurity separation test was conducted to verify whether the high-voltage electrostatic membrane impurity separation device can achieve the expected effect. The main indicator of the high-voltage electrostatic separation test is the separation rate of residual membrane and impurities. The required samples were prepared with the size distribution of the residual film, and the membrane impurities separation device was used as the test equipment. In addition, the static voltage level of the device, the height of the electrode plate, the size of the residual film, and the speed of the motor were selected through the separation principle of high-voltage electrostatic and the literature review factor.

The following four influencing factors were respectively analyzed and verified by the single-factor level test to determine the better indicators, thus providing data support for subsequent regression experiments and analysis. According to the characteristics of the device and the distribution of the residual film in the Xinjiang soil, the factor level table shown in Table 3 is determined. The static voltage level is 55 kV, the height of electrode plate is 80 mm, the size of the residual film is 17-25 cm^2, and the rotation speed of separation roller is 30 r/min. When the other three factors are at 0 level, the influence of each single-factor change on the separation rate of the device is tested.

Table 3. Single factor test factors horizontal table

Level	Factor			
	Static voltage level(kV)	**Electrode plate height(mm)**	**Residual film size(cm²)**	**Motor speed(r/min)**
1	30	60	1~4	20
2	35	70	5~9	25
3	40	80	10~16	30
4	45	90	17~25	35
5	50	100	26~36	40
6	55		37~49	
7	60			

Through the single-factor test, the optimal level interval of four test factors was obtained. The static voltage level was 50-60 kV; the height of the electrode plate was 70-90 mm; the sizes of the residual films were 16, 20, and 25 cm^2; and the electrode rotation speed levels were 25, 30, and 35 r/min. The response surface experimental design was carried out with the separation rate of the residual film and impurities as the index. The table of test factor levels is shown in Table 4.

Table 4. Regression test factor level

Level	Factor			
	Static voltage level(kV)	**Electrode plate height(mm)**	**Residual film size(cm²)**	**Motor speed(r/min)**
1	50	70	16	25
0	55	80	20	30
-1	60	90	25	35

3. Results analysis

3.1 Analysis of simulation test results

3.1.1 Influence of different electrostatic levels between electrode plates on electric field distribution

The simulation selected three different static voltage levels between the two electrode plates. The static voltage levels of the left electrode plate were 50, 55, and 60 kV, respectively, and the right side was 0 kV. The distance between the electrode plates was 80 mm, the thickness of the electrode plates was 200 mm, and the width of the electrode plates was 200 mm. The simulation results are shown in Fig. 4.

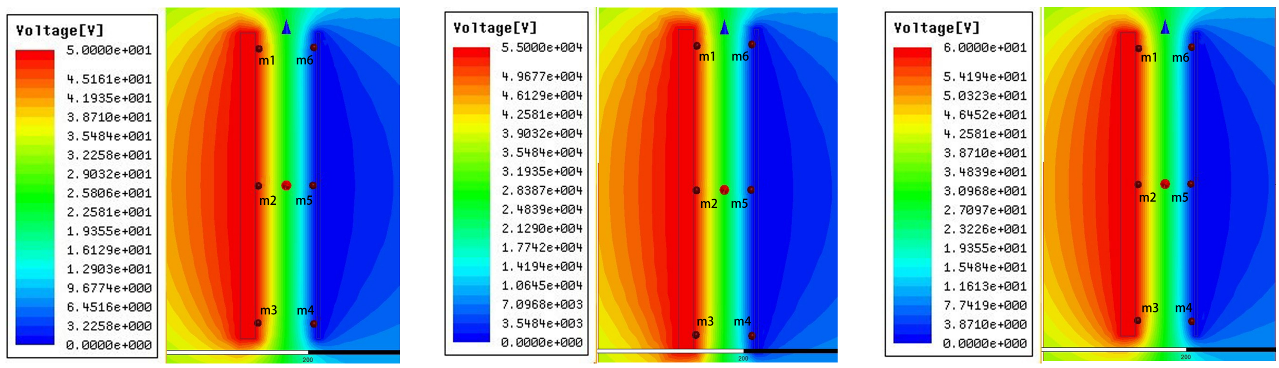

(a) (b) (c)

Fig. 4. The optimal distribution map of different static voltage levels. (a) 50 KV (b) 55KV (c) 60 KV

The figure shows the electric field strength and vector distribution between the two electrode plates at different electrostatic voltage levels. According to the simulation results, the electric field distribution of 50-60 kV is relatively uniform, the electric field vector trend is relatively regular, and the vectors all point to the right electrode plate. From m1-m6 in the figure, the electrostatic voltage levels of the electrode plate at different points can be obtained. When the static voltage level is 50-60 kV, the voltage distribution on the electrode plate is the most uniform and stable.

3.1.2 Influence of different distances between electrode plates on electric field distribution

The simulation selected three different distances between the two electrode plates, which were 70, 80, and 90 mm. The static voltage level of the left electrode plate was 55 kV, and the right side was 0 kV. The thickness of the electrode plate was 20 mm, and the width of the electrode plate was 200 mm. The simulation results are shown in Fig. 5.

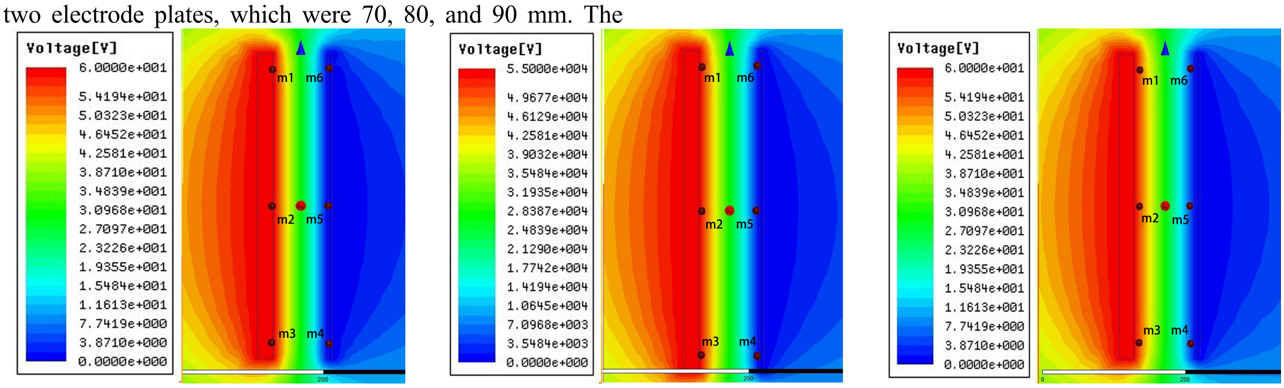

(a) (b) (c)

Fig. 5. The optimal distribution map of different distances. (a) 70 mm (b) 80 mm (c) 90 mm

The figure shows the electric field strength and vector distribution under different charging distances between the two electrode plates. According to the simulation results, when the distance is 60 mm, the distribution of electric field vector is chaotic, and the arc can easily occur during the test, which is dangerous. When the distance is 70-90 mm, the voltage distribution on the electrode plate is more uniform, and the electric field vector trend is more regular. When the distance is 100 mm, the voltage near the right electrode plate is smaller. When the distance between the electrode plates is 70-90 mm, the voltage distribution on the electrode plates is most uniform and stable.

3.1.3 Effects of different thicknesses of electrode plate on electric field distribution

The simulation selected three different electrode plate thicknesses: 10, 20, and 30 mm. The static voltage level of the left electrode plate was 55 kV, and the right side was 0 kV. The width of the electrode plate was 200 mm, and the charge distance between the electrode plates was 80 mm. The simulation results are shown in Fig. 6.

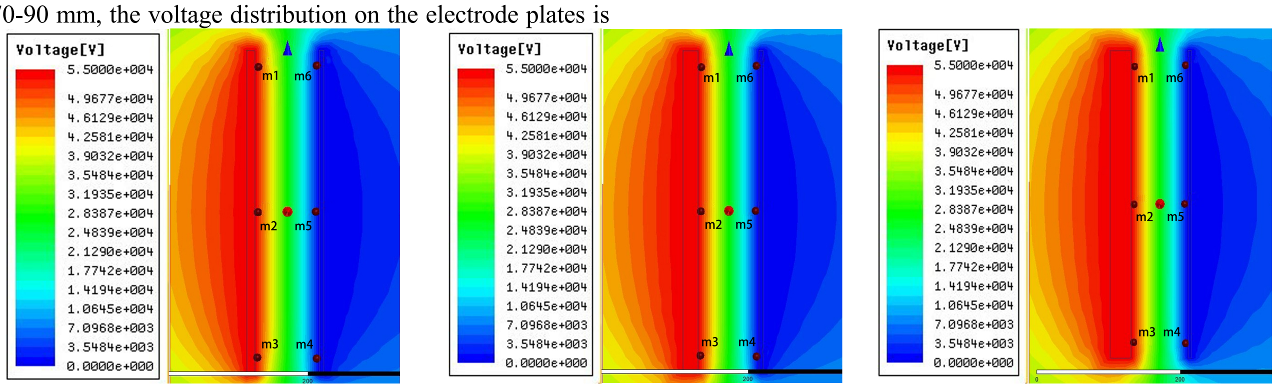

(a) (b) (c)

Fig. 6. The optimal distribution map of different thickness. (a) 10 mm (b) 20 mm (c)30 mm

The figure shows the electric field intensity and vector distribution under the condition of different thickness of the electrode plate. According to the simulation results, when the thickness of the electrode plate is 10 mm, the vector arrow on the right side is red, and the voltage level is 55 kV. This indicates that the electrode plate responsible for charging is too thin and the voltage attenuation is small, which directly punctures the right electrode plate. When the thickness of the electrode plate is 30 mm, the voltage distribution on the right electrode plate is too small. When the thickness of the electrode plate is 20 mm, the voltage on the right electrode plate is relatively uniform.

3.1.4 Influence of different widths of electrode plates on electric field distribution

We used 3D modeling for the simulation of the electrode plate width, and three values were selected for the width of the electrode plate: 100, 200, and 300 mm. The static voltage level of the upper electrode plate was 55 kV, and the lower side is 0 kV. The thickness of the electrode plate was 20 mm, and the charge distance between the electrode plates was 80 mm. The simulation results are shown in Fig. 7.

The figure shows the voltage cloud diagram and electric field vector simulation when the width of the electrode plate is 200 mm. As can be seen, the electric field vectors are mainly concentrated in the middle of the electrode plate. Furthermore, the surrounding vectors are less distributed and attenuated, and the surrounding vectors are generally close to the lower electrode plate. When the width of the electrode plate is 100 mm, the charging time of the membrane-stubble mixture on the separation roller is shorter. When the width of the electrode plate is 200 mm, the electrifying time is too long, which may cause impurities in the membrane-stubble mixture to adsorb on the separation roller and affect the separation rate of the membrane stubble.

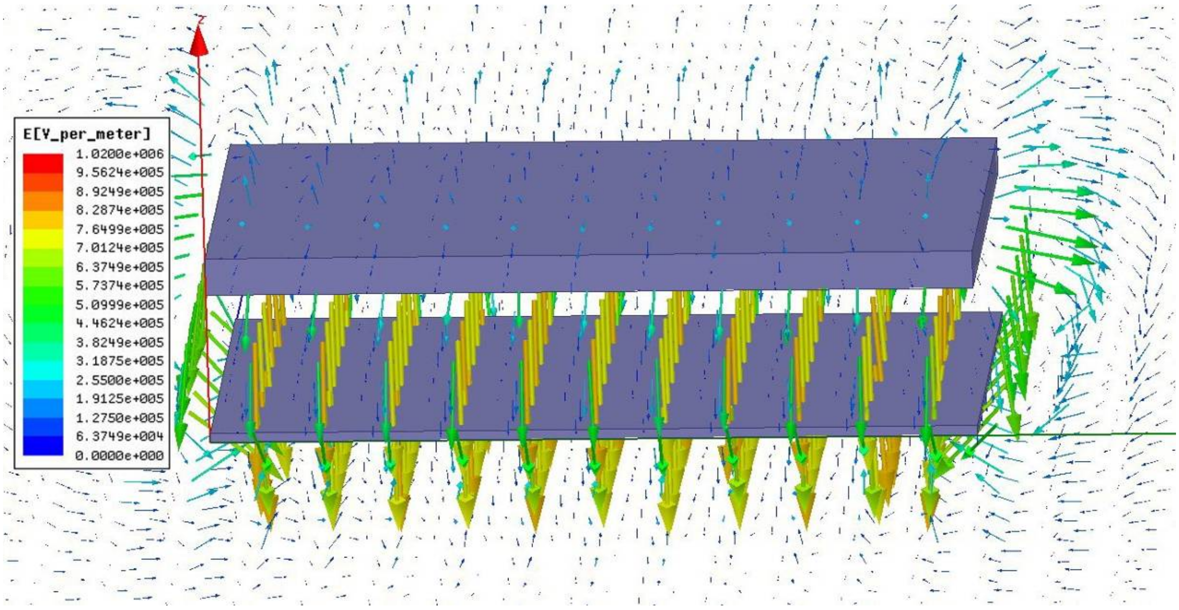

(a)

(b)

Fig. 7. 200 mm the optimal distribution map of width. (a) Electric field vector distribution (b) Voltage nephogram

3.2 Test results and analysis

The response surface test was conducted, with different static voltage levels, electrode plate heights, residual film sizes and motor speed as test factors. The actual separation efficiency was used as an index to obtain the test results of the response surface.

Design expert 10 was used to fit the test data, and the regression equation of the static voltage level, electrode plate height, residual film size and electrode rotation speed on the impurity removal rate of the device were obtained as shown in the equation:

$$\begin{aligned}\omega = {} & 80.97 - 1.73A - 0.58B - 0.84C + 1.39D - 0.55AB - \\ & 1.30AC - 5.71AD - 4.22BC - 0.18BD + 2.28CD - \\ & 15.34A^2 - 7.36B^2 - 4.23C^2 - 5.24D^2 + 12.92ABC - \\ & 13.49ABD - 10.40ACD - 0.71BCD - 9.56A^2B + \\ & 5.19A^2C + 3.78A^2D + 6.58AC^2 + 2.55B^2C - 1.40B^2D + \\ & 1.20BC^2 - 3.37C^2D + 2.08CD^2\end{aligned} \tag{3}$$

where A represents the static voltage level, kV; B represents the height of the electrode plate, mm; C represents the size of the residual film, cm^2; and D represents the motor speed, r/min.

To more intuitively reflect the effects of device removal under different influencing factors, according to the secondary regression model in Equation 3, the corresponding surface optimization model is obtained, as shown in Fig. 8.

Figs. 8a, b, c, d, e, and f are the response surface diagrams of the interactions of the four influencing factors (static voltage level, motor plate height, residual film size, and motor speed) on the impurity removal rate. It can be seen from Fig. 8a that when the size of the residual film and the motor speed are 20.5 cm^2 and 30 r/min, respectively, at the “0” level, the separation efficiency increases first and then decreases with the increase of the static voltage level and the height of the electrode plate. In Fig. 8b, when the height of the electrode plate and the motor speed are 80 mm and 30 r/min, respectively, at the “0” level, the separation efficiency increases first and then decreases with the increase of the static voltage level and the size of the residual film. In Fig. 8c, when the size of the residual film and the height of the electrode plate are 20.5 cm^2 and 80 mm, respectively, at the “0” level, the separation efficiency increases first and then decreases rapidly with the increase of the motor speed and the static voltage level. It shows that when the speed of the separation roller is too fast, the separation efficiency decreases accordingly, which has a great impact on the separation efficiency.

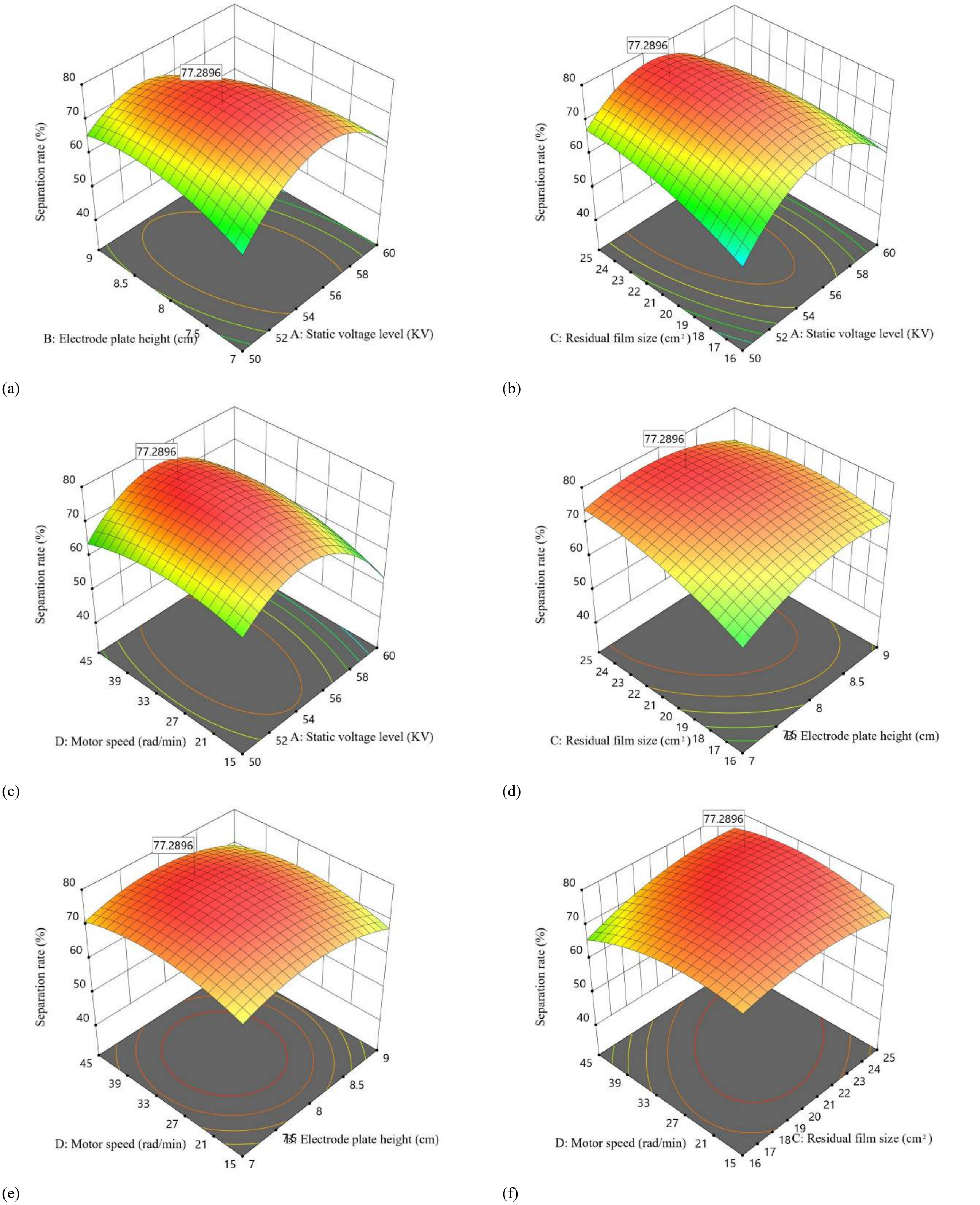

Fig. 8. The corresponding curved surface and equivalent of each factors to the device separation rate. (a) A、B corresponding surface (b) A、C corresponding surface (c) A、D corresponding surface (d) B、C corresponding surface (e) B、D corresponding surface (f) C、D corresponding surface

As shown in Fig. 8d, when the motor speed and static voltage level are 30 r/min and 55 kV, respectively, at the “0” level, the separation efficiency increases first and then decreases rapidly with the increase of the residual film area and electrode plate height. It shows that the size of the residual film area and the charging distance of the electrode plate have a great influence on the separation efficiency. In Fig. 8e when the motor speed and electrode plate height are 30 r/min and 80 mm at the "0" level, the separation efficiency first rises and then slowly decreases with the increase of motor speed and electrode plate height. It shows that the influence of motor speed and electrode plate height is weaker than the static voltage level on separation efficiency. Finally, it can be seen from Fig. 8f that when the static voltage level and the height of the motor plate are 55 kV and 80 mm, respectively, at the “0” level, the separation efficiency first increases rapidly and then decreases slowly with the increase of the motor speed and the residual film area.

Combined with contour lines, response surface maps, and the interaction between the four factors, the optimization function in Design-Expert® was used to optimize the residual film separation rate, and the following optimal parameters were obtained: static voltage level of +54.60 kV, 78.8 mm distance between the plate and the separation roller, residual film area of 21.75 cm^2, and the rotation speed of the separation roller set at 31.30 r/min. At this time, the separation rate of the device is 79.15%, which is good for the film-stubble mixture recovered by the separation machine. Thus, the separation effect meets the requirements of residual membrane separation and secondary utilization.

3.3 Operational performance verification test

To verify the actual separation rate of the optimized parameter separation device, a verification test was carried out according to the optimized parameters. The static voltage level of the separation device was set to +54.60 kV, the distance between the electrode plate and the separation roller was 78.8 mm, and the speed of the separation roller was 31.30 r/min. Then, we adjusted the pulverizing device to control the residual film area to be between 16-25 cm^2, after which we conducted five groups of repeated tests and calculated the test results by the average value. The test results of the prototype are shown in Table 5.

Table 5. Sample machine performance verification test results

Serial number	Separation rate of residual membrane (%)	Impurity content of residual membrane after separation (%)
1	77.89	1.14
2	78.95	0.98
3	79.13	0.77
4	81.08	1.25
5	77.56	0.59
Average value	78.92	0.95

Repeated tests were conducted through the optimal parameters, and the test results showed that the highest and lowest residual membrane separation rates were 81.08% and 77.56%, respectively. The average recovery rate of residual film was 78.92%. Compared with the predicted results, the error is small, and the test results are basically consistent. The average impurity content of the residual membrane after separation is 0.95%, which has little influence on the secondary recycling process of the residual membrane.

4. Discussion

4.1 Analysis of the charging capacities of different residual films

When the charging test was carried out on the residual films of different sizes, with the increase of the static voltage level, the surface charge of the mulch films also increased accordingly. Furthermore, the static voltage level was found to be the main factor affecting the residual film’s charging ability. When the residual film area is less than 9 cm^2, the residual film area is small, the dielectric polarization ability is limited, and the measurement results are relatively unstable; however, the charge capacity is still rising with the increase of the static voltage level. When the area of the residual film is between 17-25 cm^2 and the distance is 80 mm, the rising trend of the charge on the film is relatively stable. At this time, the area of the residual film is moderate. According to the area distribution of the crushed residual film, it can be known that the residual film of 17-25 cm^2 accounts for about 1/2 of the total amount of the crushed residual film, which is conducive to obtaining a stable charge on the residual film during separation and improving the separation efficiency.

At the same time, the charging capacity of the new and old mulching film is compared. As shown in Fig. 9, the trend of the surface static voltage level of the mulching film is the same as that of the old mulching film. However, because the shape and pores of the old film are different from those of the new film, the surface static voltage of the former is not as stable as that of the latter, although the difference in charge is small. It can be found that the influence of the new film on the surface static voltage of the film is small, and the trend of charge is the same.

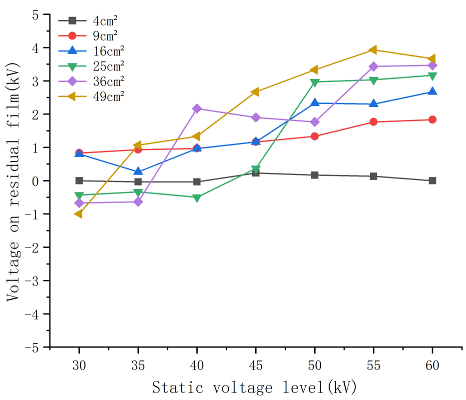

(a)

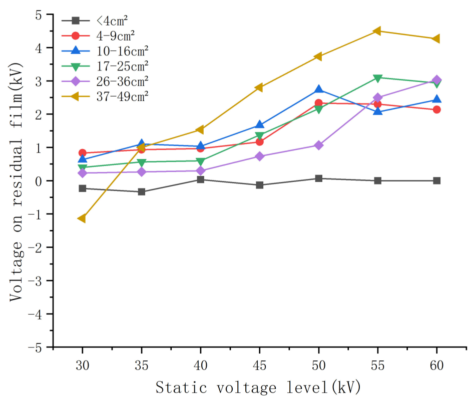

(b)

Fig. 9. Surface charge of new and old mulching film. (a) New mulching film (b) Old mulching film

4.2 Analysis of factors affecting the separation efficiency of the unit

The static electric field between the separation roller and the electrode plate in the process of electric field simulation was analyzed and simplified to a certain extent. The separation roller may has a certain impact on the adsorption electric field during its movement, and the impact will increase with the acceleration of the rotation speed of the separation roller. However, in the separation, the rotation speed of the separation roller is slow, and the movement process may not cause great disturbance to the adsorption electric field. Therefore, the static electric field was used for the simulation analysis of the separation process.

In the separation, the increase of the static voltage level has a significant impact on the charge of the residual film, which directly affects the separation efficiency of the device. With the improvement of the static voltage level, the static voltage on the surface of the residual film is on the rise as a whole. When the voltage is between 30 and 45 kV, the static voltage on the surface of the residual film is in the rising stage. It is basically stable at 50-60 kV, which may be due to the limited area of the film. Furthermore, the charge of the film is stable at the electrostatic voltage of 50-60 kV. Excessively high voltage will cause more adsorbed impurities and increase energy consumption. Thus, controlling the static voltage level between 50 kV and 60 kV can achieve the best separation effect.

Apart from the four factors mentioned in the test (i.e., the static voltage level, the height of the electrode plate, the size of the residual film, and the rotation speed of the separation roller), other factors, such as the type of the residual film, the shape of the broken residual film, and the curling degree of the residual film, may also affect the device parameters at the time of optimal separation. However, these factors do not offer convenience when it comes to regulating the actual separation process, and it is observed that these factors have no significant effects on the separation rate. Thus, from the perspective of engineering application, these factors need not be added to the test.

5. Conclusion

To address the problem involving the difficulty of recycling residual films after mechanical recovery, this study takes the residual film and impurities after preliminary processing and crushing after mechanical recovery as its research objects (including fine sand and the root of the cotton stalk after crushing) and investigates them according to high-voltage electrostatic separation. Based on the theory, the electric field distribution of the separation device was analyzed, and a regression experiment was designed to determine the influence of different factors on the separation rate of the device. The following conclusions were drawn:

(1) The surface electrostatic voltage and spatial electric field distribution of the residual film directly affect the separation efficiency of the separation device.

(2) The simulation found that the electrostatic voltage level, the distance between the electrode plate and the separation roller, the charged area of the electrode plate, and the fragmentation degree of the residual film all had significant effects on the surface electrostatic voltage of the film and impurities and the spatial electric field distribution.

(3) Increasing the applied static voltage level and reducing the distance between the electrode plate and the separation roller can significantly improve the separation rate of the separation device.

This study combines experiment and simulation analysis to study the relationship between different influencing factors and the separation efficiency of the proposed device. The experimental results show that the average residual membrane recovery rate of the device is 78.92% under the optimal parameters. Furthermore, the average impurity content of the residual membrane after separation is 0.95%, which meets the requirements of the secondary recycling of the residual membrane. Therefore, it can help with the recovery and treatment of the residual membrane pollution.

Acknowledgements

The authors would like to acknowledge the financial support by the Bintuan Science and Technology Program (Grant No.2020CB028), the National Natural Science Foundation of China (Grant No. 32060288), and the National Natural Science Foundation of China (Grant No. 32160300).

References

1. Bi J., Wang X., Zhu D. “The effect of plastic film mulching on crop yield,” *Chinese Journal of Agricultural Engineering*, 24(11), 2008, pp.172-175.
2. Chen Q., “China's Plastic Film Covering Agriculture,” *China Engineering Science*, 02(12), 2002, pp.12-15.
3. Ma F. , Zhou Z., Zheng Z., Zheng X., Li M., Li Z., Zhang W., Xing M., Xia D., “Development and Improvement of Drip Irrigation Technology for Cotton in Xinjiang,” *Agricultural Research in Arid Areas*, 22(3),, 2004 pp.202-208.
4. Weihua, Z., Hao, H., Fenfang, T., Hong, W., Rongliang, Q., “Influence of EDTA washing on the species and mobility of heavy metals residual in soils,” *Journal of Hazardous Materials* , 173(1), 2010, pp.369-376.
5. Xu X. , Hu H., Chen Y.,“Effects of polyethylene microplastics on soybean growth,” *China Soil and Fertilizer*, 21(6), 2021, pp.262-268.
6. Ruijie, L., Lianzhen, L., Yunchao, Z., Jie, Y., Chen, T., Qian, Z., Yuan, L., Yongming, L., “Uptake and accumulation of microplastics in a cereal plant wheat,” *Chinese Science Bulletin* , 65(20), 2020, pp.2120-2127.
7. Ding F., Luo X., “*Basic study on the separation and environmental degradation characteristics of plastic film microplastics in soil*.” Master thesis of Southwest University of Science and Technology, China, 2021. pp.23-28.
8. Ministry of Agriculture and Rural Affairs of the People's Republic of China “The Ministry of Agriculture’s Notice on Printing and Distributing the Action Plan for the Recycling of Agricultural Films.” [EB/OL]. Retrieved from https://www.moa.gov.cn/nybgb/2017/dlq/201712/t20171231_6133712.htm, 2017-06-20/2022-08-06.
9. Hou S., Hu S., Kong J., Zhang H., Na M., Dong X., “Research Status of Domestic Residual Film Recycling Machine,” *Chinese Journal of Agricultural Engineering*, 22(03), 2022, pp.186-190.
10. Wen H., Ji T., Chen X., “Development of a second-order chain plate type straw crushing and plastic film recycling combined working machine,” *Agricultural Development and Equipment*, 21(07), 2021, pp.40-41.
11. Jin W., Bai S., Zhang X., Zhou X., Ma S., “Parameter optimization and experiment of spring-tooth type residual film recovery machine,” *Agricultural Mechanization Research*, 42(09), 2020, pp.186-190.

12. Du T., Song L., Luo S., Zhao Y., "Analysis of the current situation of waste plastic film recycling and related standards in China," *Renewable Resources and Circular Economy*, 13(05),2020, pp.24-26.
13. Shu F., "*Research on the utilization and recycling of agricultural plastic film in China and its financial support policy*." Master thesis of Chinese Academy of Agricultural Sciences, China, 2014, pp.35-38.
14. Karim, M., Ahlem, B., Tahmi, Z., Lucien, D., "Recent trends in recycling and reusing techniques of different plastic polymers and their composite materials," *Sustainable Materials and Technologies* , 22(31), 2022, pp. 00382.
15. Chang, L., Mingxing, S., Xiangbo, X., Linxiu, Z., Jianbing, G., Yuhan, Y., "Environmental village regulations matter: Mulch film recycling in rural China," *Journal of Cleaner Production* , 21(299), 2021, pp. 126796.
16. Liang R., Chen X., Zhang B., Meng H., Jiang P., Peng X., Kan Z., Li W., "Recycling methods of residual film in Xinjiang cotton fields and the current situation and countermeasures of resource recycling," *Chinese Journal of Agricultural Engineering*, 35(16), 2019, pp.1-13.
17. Adrian, S., Lucian, D., Laur, C., Mihai, B., Andrei, C., "Recent researches in electrostatic separation technologies for the recycling of waste electric and electronic equipment," *AIP Conference Proceedings* , 2018(1), 2020, pp. 030001.
18. Silveira, A. V. M., Cella, M., Tanabe, E. H., Bertuol, D. A., "Application of tribo-electrostatic separation in the recycling of plastic wastes," *Process Safety and Environmental Protection* , 18(114), 2018, pp.219-228.
19. Rezoug, M., Seddik, T., Boukhoulda, M. F., Wessim, A., Karim, M., Lucian, D., "New Spiral-type Tribocharger for Granular Plastics Mixtures with Application to Electrostatic Separation." *2021 IEEE Industry Applications Society Annual Meeting*, Virtual: IEEE, 2021, pp.1-4.
20. Tahsin Onur, D., Gizem, K., Ergin, G., Özcan, Y. G., "A new method to produce high voltage static electric load for electrostatic separation-Triboelectric charging," *Powder Technology*, 18(327), 2018, pp.89-95.
21. Gontran, R., Abdelhady, S., Karim, M., Thami, Z., Lucian, D., "Comparative study of three high-voltage electrode configurations for the electrostatic separation of aluminum, copper and PVC from granular WEEE," *Journal of Electrostatics*, 17(88), 2017, pp.29-34.
22. Kawamoto, H., "Some techniques on electrostatic separation of particle size utilizing electrostatic traveling-wave field," *Journal of Electrostatics*, 66(3), 2008, pp. 220-228.
23. Karim, M., Ahlem, B., Tahmi, Z., Lucien, D., "Influence of Particle Size after Grinding in Electrostatic Separation of Granular Plastic Mixtures," *International Journal of Electronics and Electrical Engineering Systems*, 3(4), 2020, pp.23-28.
24. Dorota, C.-K., Cezary, J., Dariusz, S., Roman, R., Krzysztof, N., Dominik, R., Mariusz, B., Mateusz, B., "Concept and Design of the Test Bench for Electrostatic Separation in Plastic Recycling Application," *MATEC Web of Conferences*, 22(357), 2022, pp. 04005.
25. Hamza, L., Rabah, O., Noureddine, Z., Amar, T., "Numerical and Experimental Analysis of the Electrostatic Separation of a Metal/Polymer Mixture Based on Electro-Adhesive Force," *IEEE Transactions on Industry Applications*, 58(1), 2022, pp.760-766.
26. Koichi, T., Nobuya, H., Douyan, W., Takayuki, O., "High-voltage technologies for agriculture and food processing," *Journal of Physics D: Applied Physics*, 52(47), 2019, pp. 473001.
27. Ahmed, T. Kourmatzis, A., Masri, A. R., "Atomization behaviour of a hybrid air-blast-electrostatic atomizer for spray combustion," *Fuel*, 21(288), 2021, pp. 119716.
28. Dipak, S. K., Shaji, P. J., Dhalin, D., "Role of electrostatics in artificial pollination and future agriculture," *CURRENT SCIENCE*, 120(3), 2021, pp. 8.
29. Julián, S. H., José, P. A., Patricio, M. C., Fernando, C. R., Francisco, A. V., "Evaluation of Electrostatic Spraying Equipment in a Greenhouse Pepper Crop," *Horticulturae*, 8(6), 2022, pp. 541.
30. Lucian, D., Ciprian, D., Mihai, B., Radu, B., Youna, H., Xavier, R., "Electrostatic Basis for Separation of Wheat Bran Tissues," *IEEE Transactions on Industry Applications*, 46(2), 2010, pp.659-665.
31 Jue, W., Jun, Z., Martin de, W., Remko, M. B., Maarten, A. I. S., "Lupine protein enrichment by milling and electrostatic separation," *Innovative Food Science & Emerging Technologies*, 16(33), 2016, pp.596-602.
32. Wang J., Zhao W., Liu X., Dai F., Xin S. Wu Z., "Optimal Design and Experiment of Recycling Machine for Corn Full Film Double-furrow Residual Film," *Journal of Agricultural Machinery*, 52(01), 2021, pp.119-128.
33. Zhou L., Shi A., Shi Q., Ding J. Lu J., Li D., "Parameter optimization and experiment of combined residual film recovery machine with upper conveyor tooth chain," *Agricultural Mechanization Research*, 45(04), 2022, pp.164-170.
34. Ma X., Zhang H., Wang X., Liao J., Zhao J., "Development and test of cotton film residue recovery machine in southern Xinjiang," *Agricultural Mechanization Research*, 44(05), 2022, pp.72-77.